

# Ripple topography on thin ZnO films by grazing and oblique incidence ion sputtering

S. Bhattacharjee<sup>1</sup>, P. Karmakar<sup>2\*</sup>, V. Naik<sup>2</sup>, A. K. Sinha<sup>1</sup> and A. Chakrabarti<sup>2</sup>

<sup>1</sup>UGC-DAE CSR, Kolkata Centre, III / LB -8, Saltlake, Kolkata 700 098, India

<sup>2</sup>Variable Energy Cyclotron Centre, 1/AF, Bidhannagar, Kolkata 700 064, India

## Abstract

We have investigated the formation and growth of nano sized ripple topography on ZnO thin films by 10 keV O<sup>1+</sup> bombardment at impact angles of 80° and 60°, varying the ion fluence from  $5 \times 10^{16}$  to  $1 \times 10^{18}$  ions/cm<sup>2</sup>. At 80° the ripples are oriented along the ion beam direction whereas at 60° it is perpendicular to the ion beam direction. The developed ion induced structures are characterized by Atomic Force Microscopy (AFM) and the alignment, variation of rms roughness, wavelength and correlation length of the structures are discussed with the existing model and basic concept of ion surface interaction.

PACS number: 61.80.Jh, 81.16.-c, 79.20.Rf, 81.16.Rf, 79.20.Ap

---

\*Corresponding author, E-mail: [prasantak@vecc.gov.in](mailto:prasantak@vecc.gov.in)

## 1. Introduction

Nanostructure formation on crystalline and amorphous solids using ion bombardment has become a topic of rapidly increasing interest. The use of low energy ion beams for this purpose allows a precise control on morphology, size and composition of the nano structures [1]. ZnO nanostructures have been put to a wide range of application ranging from field emission sources to optical devices such as solar cells, efficient blue light emitters etc [2] as well as it is an environment-friendly material. A variety of ZnO nanostructures including nanowires, nano needles, nano rods, nano helices and nano belts have been synthesized by a variety of techniques such as molecular beam epitaxy (MBE), thermal evaporation, vapour phase transport, sputter deposition and laser ablation [2]. The use of low energy ion beams for the fabrication of controlled zinc oxide nanostructures could be an attractive and cost effective way.

In the present work we have formed nano structures on ZnO thin film deposited on Si(100) substrate by 10 keV  $^{16}\text{O}^{1+}$  bombardment at impact angles of  $80^\circ$  and  $60^\circ$ , varying the ion fluence. It is observed that ripple structures are developed both in grazing and oblique angle incidence. At grazing incidence, the ripples are oriented along the ion beam direction whereas at oblique incidence they are rotated by  $90^\circ$ . The formation mechanism and orientation of the ripples are correlated with the fundamentals of angle dependent ion surface interaction.

## 2. Experimental

Thin films of about 115 nm thick ZnO were deposited by d.c. magnetron sputtering on clean Si(100) substrates. Prior to the deposition the Si(100) substrates were cleaned and degreased in ultrasonic bath. The samples were bombarded with mass

analyzed 10 keV  $^{16}\text{O}^{1+}$  ions at incidence angles of  $80^\circ$  and  $60^\circ$  with respect to the surface normal. The ion beam was extracted from the 6.4 GHz ECR ion source of the Radioactive Ion Beam Facility at Variable Energy Cyclotron Centre Kolkata [3]. To investigate the evolution of the surface morphology the fluence was varied over a wide range from  $5 \times 10^{16}$  ions/cm<sup>2</sup> to  $1 \times 10^{18}$  ions/cm<sup>2</sup>. The irradiated samples were examined in air using Atomic Force Microscopy (AFM) (Nanoscope IV digital instrument) in contact mode and the data are analyzed by WSxM code [4]. For the quantitative analysis of the surface morphology we have calculated the rms roughness  $w$ , correlation length  $\xi$  and ripple wavelength  $\Lambda$  from the AFM data. The rms roughness  $w$  is a measure of height amplitude and correlation length  $\xi$  is the measure of lateral dimension of the nanostructures. Ripple wavelength  $\Lambda$  is defined as the lateral distance between two ripples [5,6] .

### 3. Results and Discussion

The surface morphologies and dynamics of the morphology as a function of ion fluence for the  $60^\circ$  and  $80^\circ$  incidence angles are shown in Fig.1. The AFM image of the unbombarded ZnO film is shown in Fig.1(a) whereas Fig.1(b) shows the morphology of the samples after the bombardment with ion fluence of  $5 \times 10^{17}$  ions/cm<sup>2</sup> at oblique incidence where the ripple structures are formed in the direction perpendicular to the ion beam direction. Similarly, Fig.1 (c) shows the AFM images and dynamics of the morphology with ion fluence of  $1 \times 10^{18}$  ions/cm<sup>2</sup> for the grazing angle ( $80^\circ$ ).

For the quantitative estimation of the surface morphology the rms roughness  $w$ , correlation length  $\xi$  and ripple wavelength  $\Lambda$  have been calculated from the AFM data. The rms roughness or the interface width ' $w$ ' at each fluence was obtained from

$w^2 = \langle (h(r) - \bar{h})^2 \rangle$  and lateral correlation length ‘ $\xi$ ’ is determined from the auto correlation function  $c(r) = \langle h(r)h(0) \rangle$ , where  $h(r)$  is the relative surface height at the position  $r$ ,  $\bar{h}$  is average surface height and  $\langle \rangle$  denotes an average over all positions and directions.  $\xi$  is defined as the value of  $r$  at which  $c(\xi) = c(0)/e$ , where  $e$  is the base of the natural logarithm [5]. Plotting the 1D-autocorrelation function along the wave vector of the ripple structure for  $60^\circ$  and  $80^\circ$  incidence shows well-defined satellites due to the periodicity of the rippled surface. The mean ripple wavelength is defined as the separation between the central peak and the first secondary correlation maximum [6]. Fig.2 (a) and 2 (b) shows the experimental results of the fluence ( $\varphi$ ) dependence of surface roughness ( $w$ ) for  $60^\circ$  and  $80^\circ$  incidence angle respectively. It shows fast initial rise of rms roughness with ion fluence which is in qualitative agreement with B.H. theory [7] that predicts exponential increase of rms roughness with ion fluence. The linear fit to the data in the growth part by an function  $w \sim \varphi^\beta$  gives the value of the exponent for the ascending part of the roughness curve,  $\beta_1 = 0.327 \pm 0.07$  and  $\beta_2 = 0.323 \pm 0.03$  for  $60^\circ$  incidence and  $80^\circ$  incidence respectively, where  $w$  is the rms roughness,  $\varphi$  is fluence and  $\beta$  is known as the growth exponent. It is interesting to note that with the further increase of the ion fluence the roughness decreases due to the erosion of the film material. Theoretical calculations, considering the value of sputtering yield  $\sim 8$  from TRIM [8] for 10 keV  $O^{1+}$  on ZnO/Si surface showed that the film material will be completely eroded at fluence  $1 \times 10^{17}$  ions/cm<sup>2</sup> but in practice due to simultaneous interface mixing and recoil implantation the ZnO film will not be totally eroded and small fraction will remain there. Similar decrease of roughness with ion fluence was also seen for bombardment of Pt thin

films [6]. The value of the exponent for the descending part of the roughness curve is found to be  $\beta_1 = -1.59 \pm 0.29$  and  $\beta_2 = -1.270 \pm 0.52$  for  $60^\circ$  and  $80^\circ$  incidences respectively.

Fig.2(c) and (d) shows the variation of correlation length ( $\xi$ ) on ion fluence for  $60^\circ$  and  $80^\circ$  incidence angle respectively. In case of  $60^\circ$  incidence the variation of ripple width ( $\xi$ ) with increasing ion fluence initially remains constant and then rises sharply (Fig 2(c)). According to B.H. theory [7] the wavelength of the ripple ( $\sim \xi$ ) should be constant as is observed at lower fluence for oblique incidence. But for further bombardment it increases following the power law  $\xi \sim \phi^\gamma$  with an exponent of  $\gamma_1 = 0.539 \pm 0.18$  due to the nonlinear effect at higher ion fluence [9]. Habenicht et al. also observed similar increase of ripple width with the exponent of 0.50 [10]. Similarly in the case of  $80^\circ$  incidence, the  $\xi$  increases following the same power law with  $\gamma_2 = 0.572 \pm 0.03$  (Fig.2 (d)).

The morphology of surface evolves during ion bombardment due to the instability generated by the ion beam. The removal of atoms and the creation of adatom/vacancy pairs by the incident beam cause continuous perturbations on the surface topography. With further ion irradiation, the perturbation grows and generates structures on the surface depending on the incident ion beam parameters, beam sample geometry and temperature.

The BH model [7] or extended BH model, based on Sigmund's sputtering theory [11] describe the perpendicular ripple formation at oblique angle ( $60^\circ$ ) ion bombardment. The model assumes an ellipsoidal shape of the collision cascade with an initial perturbation present on the surface. The perturbation grows with ion bombardment and

generates local curvature. More energy from the collision cascades reaches to the concave curvature (valleys) than the convex curvatures (hills) on the surface and therefore, the preferential sputtering of the valleys generate instability. In addition to the sputtering induced instability, thermal diffusion is also considered, which is responsible for the smoothening of the surface during bombardment.

In the present case the observed perpendicular ripple formation (Fig. 1(b)) on ZnO film at  $60^\circ$  ion bombardment is consistent with the BH model and the previous experimental observations [1,12-15]. It is to be pointed out here that for initially flat surfaces, stochastic nature of ion beam generates the initial perturbation. Preferential sputtering, impurities on the surface or deliberate incorporation of initial roughness may also supply the initial perturbation and therefore, speed up the ripple formation during ion bombardment [16,17]. Here, as grown ZnO thin films has initial rough morphology, therefore, the initial perturbation is readily available, and thus ion bombardment at  $60^\circ$  leads to the formation of perpendicular ripple structure.

The parallel ripple formation (Fig.1(c)) at grazing ion incidence requires more insight in to the ion impact effects on the surface having initial surface features. Although, BH model predicts parallel ripple formation at grazing angle bombardment, the Sigmund sputtering theory which is the basis of BH model does not describe well the grazing incidence ion bombardment [7,11]. Therefore, to describe the ripple formation at grazing ion incidence, the distinctiveness of grazing ion surface interaction is to be taken in to account. For incident ion beam of energy  $E$ , the energy component perpendicular to the surface is  $E_{\perp} = E \cdot \cos^2\theta$ , where  $\theta$  is the ion incidence angle with respect to surface normal. Although  $E_{\perp}$  decreases with  $\theta$ , the sputtering yield first increases with  $\theta$  and

then decreases for  $\theta$  close to  $90^\circ$ . This is because the shape of the collision cascades changes with ion incidence angles. For 10 keV  $O^{1+}$  ion impact on ZnO surface, the projected range along the depth and radial direction is calculated by SRIM [8] and shown as a function of incidence angle in Fig.3. It is seen that with increasing  $\theta$  the longitudinal range decreases and radial range increases. The ratio (lateral/ longitudinal) which could be approximated as the aspect ratio of the collision cascade zones is about 1.5 at ion incidence angle  $80^\circ$ . Additionally, in grazing incidence the cascade remains closer to the surface resulting the maximum adatom and vacancy creation very near to the surface. Further increase of  $\theta$  reduces the value of  $E_\perp$ . If the angle of incidence  $\theta$  exceeds a critical angle,  $E_\perp$  become so small that energy transfer to the sample atom is no longer sufficient to initiate a collision cascade, not to sputter atoms from the surface, therefore, the ions are reflected out from the surface [9]. In case, 10 keV  $O^{1+}$  ions bombarding on an atomically flat surface at an angle  $80^\circ$ , the perpendicular energy component  $E_\perp$  is 301 eV only, therefore, most of the incident ions will either creates adatoms and vacancies on the surface along the beam direction or reflected back instead of notable sputter etching. It is also reported that elastic losses are low compared to inelastic losses at grazing angle [18]. Therefore, sputtering induced nanostructure formation at grazing angle ion bombardment on ZnO is forbidden for sample with ideally flat surface. In general, ripple formation at oblique angle is observed in a number of materials [12,14,15,19,20] while observation of parallel ripple at grazing ion bombardment with the same sample and experimental condition is very rare because of small perpendicular energy component and flatness of the sample.

In the present case, oxygen ions are bombarded on ZnO thin film at oblique ( $60^0$ ) and grazing angle ( $80^0$ ) but as grown ZnO surfaces are rough enough with grain structures on the surface. Therefore, the effective angle of impact changes with the position of impact point as shown in Fig 4. It varies from normal to grazing incidence depending upon the curvature and shape of the grains. For a hemispherical shaped grain with height  $h$  and lateral width  $2l$  the local ion impact angle  $\psi = \cos^{-1} \left[ 1 - \frac{2hr_x}{(l^2 + h^2)} \right] - \pi/2 + \theta$  where  $r_x$  is the lateral length at the point of ion impact and varies from  $r - l$  to  $r + l$ ,  $r$  being the radius of curvature of the mount and

can be calculated following: 
$$r = \frac{l^2 + h^2}{2h}$$

It is seen from the Fig. 4 that the effective ion incidence angle for  $60^0$  case, major part of the mount is bombarded at oblique angle ( $|\psi| \leq 64^0$ ) therefore, perpendicular ripples are expected. In case of  $80^0$ , the top section of the mount is bombarded at grazing angle whereas small bottom portion is either near normal or obliquely bombarded. Due to grazing ion incidence on the top portion, the adatoms and vacancies generated by ion impact will have high probability of displacement in the ion beam direction. When the generated adatoms and vacancies move on the surface in the direction of ion beam, the curvature dependent transfer of energy leads to more sputtering at the dents than the hills present on the surface [7,11]. Therefore, the combination of the displacement of adatoms and vacancy on the top surface of the mount along the ion beam direction and curvature dependent sputter erosion leads to the parallel ripple structures at grazing ion bombardment on ZnO thin film (Fig. 1(b)). Similar ripple structures along the ion beam direction were reported earlier on initially rough Si and metal surfaces [6,21,22], where,

present explanation may be applicable. Also Chan *et al.* reported parallel ripple on Cu(001) for  $70^\circ$  incidence [23] and Erlebacher *et al.* have demonstrated parallel ripple on Si samples heated at temperatures between  $400^\circ\text{C}$  and  $700^\circ\text{C}$  [24,25]. Very recently, Redigner *et al.* [26] reported the alignment of surface vacancies and adatoms along the ion trajectory for keV noble gas ions bombardment at glancing angle on Pt (111). In the present experiment it is observed that the minimum fluence required to start ripple structure is about  $5 \times 10^{16}$  ions/cm<sup>2</sup> for  $80^\circ$  incidence angle and about  $1 \times 10^{17}$  ions/cm<sup>2</sup> for  $60^\circ$ . The possible reason of early ripple formation in case of  $80^\circ$  may be due to the additional displacement of adatom/vacancy along the ion beam direction on the surface.

#### **4. Conclusion**

In conclusion, ion bombardment could produce orientation and size controlled nano ripple structures on ZnO like interesting and important material. Ripples structures are developed both in oblique and grazing angle incidence. At grazing incidence, the ripples are oriented along the ion beam direction whereas at oblique incidence it is rotated by  $90^\circ$ . Minimum fluence required to start periodic structure is less for  $80^\circ$  incidence angle compared to  $60^\circ$  incidence.

#### **Acknowledgement**

We would like to thank Prof. S. Chakrabarti for ZnO thin film deposition and Prof. D. Ghose for accessing the SPM. We also thank Mr. S. A. Mollick for active help during SPM measurements and RIB group members for constant support during ECR operation.

#### **References**

1. W. L. Chan and E. Chason, J. Appl. Phys **101** (2007).

2. V. A. Coleman and C. Jagadish, in *Zinc oxide bulk, thin films and nanostructures*, edited by C. Jagadish and S. Pearton, Elsevier 2006), p. p. 20.
3. A. Chakrabarti, Nucl. Instr. Meth. B **261**, 1018 (2007).
4. I. Horcas, Rev. Sci. Instrum **78**, 013705 (2007).
5. T. Karbacak, Y. P. Zhao, G.-C. Wang, and T. - M. Lu, Phys Rev B. **64**, 085 323 (2001).
6. P. Karmakar and D. Ghose, Surface Science **554**, L101 (2004).
7. R. M. Bradley and J. M. E. Harper, J. Vac. Sci. Technol. A **6**, 2390 (1988).
8. J. F. Ziegler, J. P. Biersack, and U. Littmark, in *The Stopping and Range of Ions in Solids* (Pergamon, New York, 1985).
9. R. Cuerno, H. A. Makse, S. Tomassone, S. T. Harrington, and H. E. Stanley, Phys. Rev. Lett **75**, 4464 (1995).
10. S. Habenicht, K. P. Lieb, J. Koch, and A. D. Wieck, Phys. Rev. B **65**, 115327 (2002).
11. P. Sigmund, Phys. Rev. **184**, 383 (1969).
12. P. Karmakar and D. Ghose, Nucl. Instr. and Meth. B **230**, 539 (2005).
13. A. Keller, S. Facsko, and W. Möller, New Journal of Physics **10**, 063004 (2008).
14. K. Zhang, F. Rotter, M. Uhrmacher, C. Ronning, H. Hofsäss, and J. Krauser, Surface & Coatings Technology **201**, 8299 (2007).
15. T. K. Chini, D. P. Datta, and S. R. Bhattacharyya, J. Phys.:Condens. Matter **21**, 224004 (2009).
16. P. Karmakar, S. A. Mollick, D. Ghose, and A. Chakrabarti, Appl. Phys. Lett. **93**, 103102 (2008).
17. P. Karmakar, G. F. Liu, and J. A. Yarmoff, Phys. Rev. B **76**, 193410 (2007).
18. M. Kato, T. Kurose, N. Inoue, T. Hasegawa, and K. Matsuzawa, Nucl. Instr. and Meth. B **67**, 316 (1992).
19. P. Mishra and D. Ghose, Physical Rev. B **74**, 155427 (2006).
20. A. Keller, S. Facsko, and W. Moller, Nucl. Instr. and Meth. B **267**, 656 (2009).
21. S. A. Mollick and D. Ghose, J. Appl. Phys. **106**, 044309 (2009).
22. S. A. Mollick, P. Karmakar, and D. Ghose, Proceedings of the DAE Solid State Physics Symposium (India) **53**, 705 (2008).
23. W. L. Chan, N. Pavenayotin, and E. Chason, Phys. Rev. B **69**, 245413 (2004).
24. J. Erlebacher, M. J. Aziz, E. Chason, M. B. Sinclair, and J. A. Floro, Phys. Rev. Lett. **82**, 2330 (1999).
25. J. Erlebacher, M. J. Aziz, E. Chason, M. B. Sinclair, and J. A. Floro, J. Vac. Sci. Technol. A **18**, 115 (2000).
26. A. Redinger, S. Standop, T. Michely, Y. Rosandi, and H. M. Urbassek, Phys. Rev. Lett. **104**, 075501 (2010).

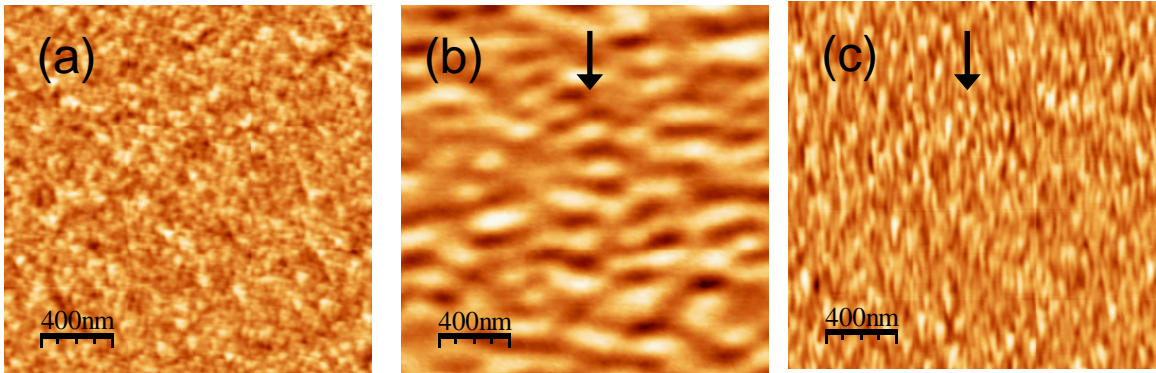
## FIGURE CAPTIONS

Fig.1. AFM images of (a) unbombarded sample, (b) bombarded at  $60^\circ$  with fluence  $5 \times 10^{17}$  ions/cm<sup>2</sup>, (c) bombarded at  $80^\circ$  with the fluence of  $1 \times 10^{18}$  ions/cm<sup>2</sup>.

Fig. 2 (a) Shows the variation of rms roughness with the ion fluence for  $60^\circ$  incidence (b) the variation of rms roughness with the ion fluence for  $80^\circ$  incidence. (c) Shows the variation of correlation length with the ion fluence for  $60^\circ$  incidence and (d) the variation of correlation length with the ion fluence for  $80^\circ$  incidence. The straight line shows the linear fit to the data points following the power law  $\xi \sim \phi^\gamma$ .

Fig.3. Variation of the longitudinal and radial range as a function of incidence angle.

Fig. 4. Variation of local ion impact angle ( $\psi$ ) with ion impact point of a mount structure of radius 'l' and height 'h' for ion incidence angle ( $\theta$ )  $60^\circ$  and  $80^\circ$ .



**Figure 1**

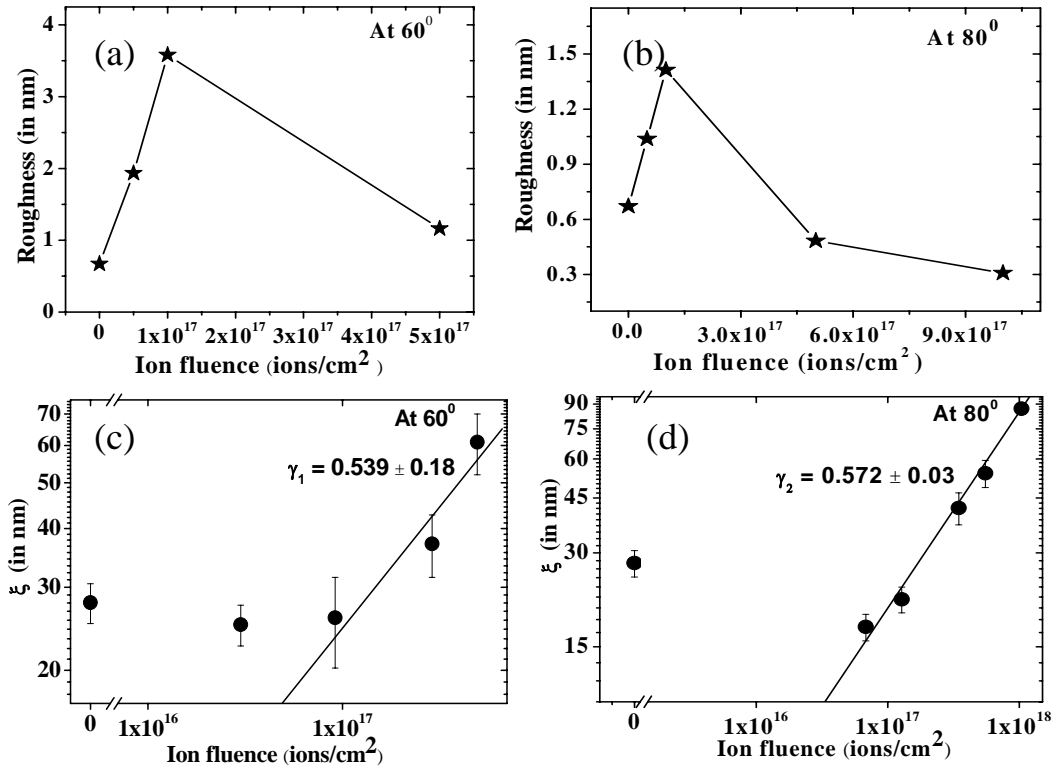
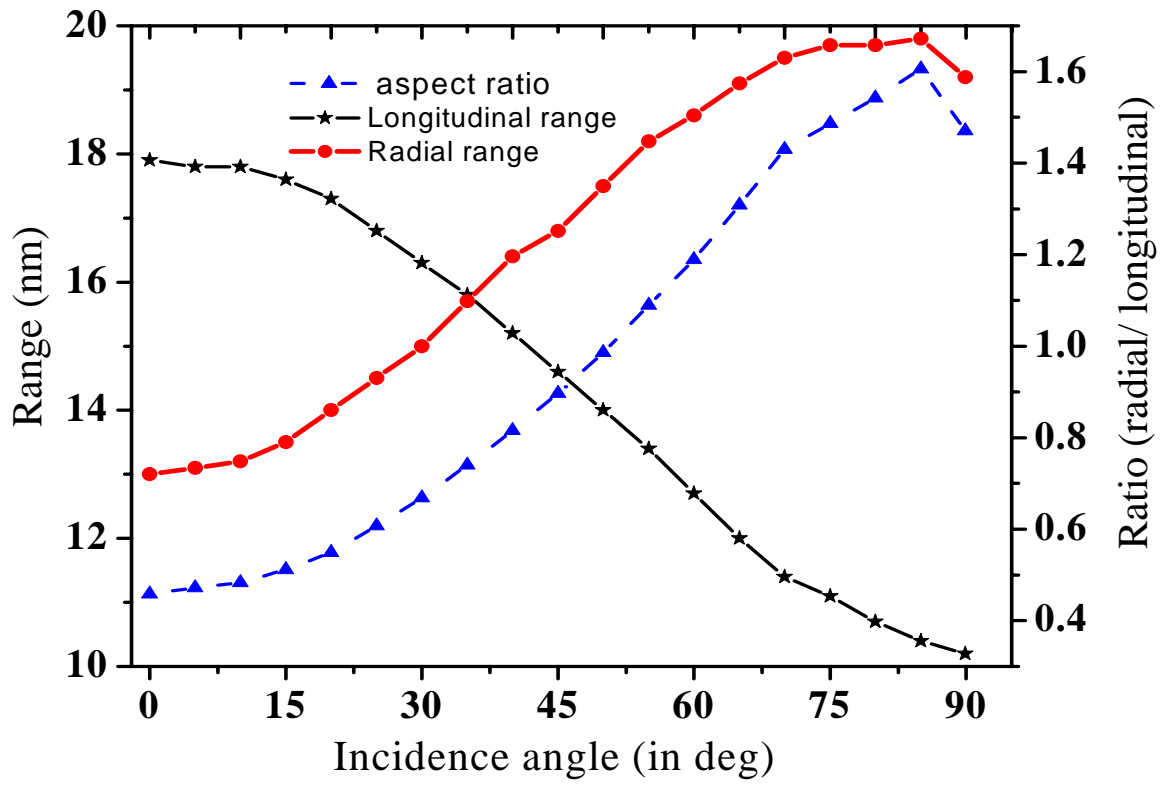
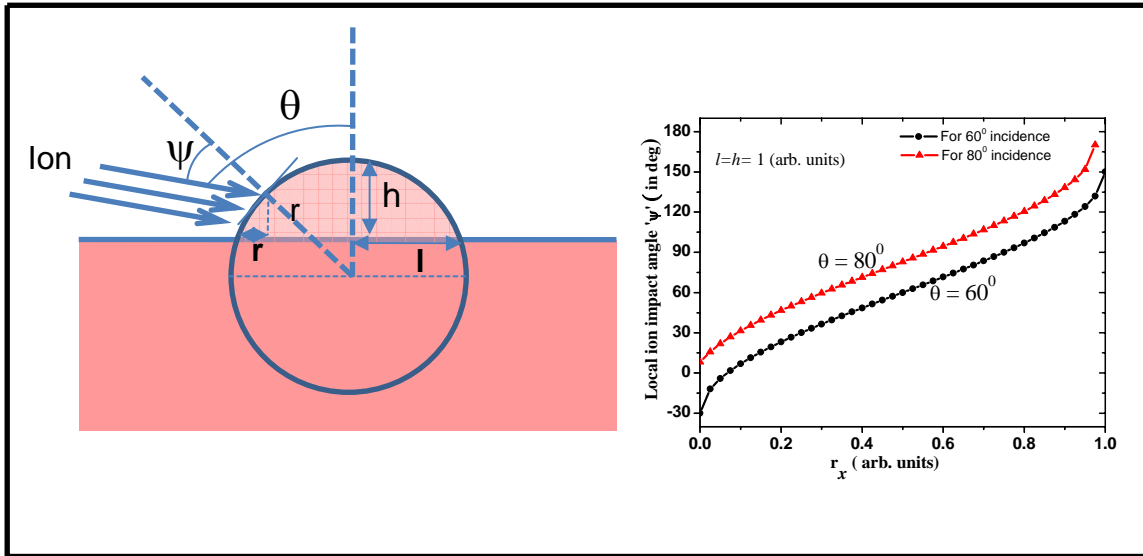


Figure 2



**Figure 3**



**Figure 4**